UCRL-CONF-232540

LAWRENCE
LIVERMORE
NATIONAL
LABORATORY

FUNCTIONALIZED LATERAL SURFACE COATED LASERS FOR CHEM-BIO DETECTION

L. L. Goddard, T. C. Bond, G. D. Cole, E. M. Behymer

July 6, 2007

IEEE Sensors Conference
Atlanta, GA, United States
October 28, 2007 through October 31, 2007

Disclaimer

Functionalized Lateral Surface Coated Lasers for Chem-Bio Detection

Lynford L. Goddard, Tiziana C. Bond, Garrett D. Cole, and Elaine M. Behymer

Center for Micro and Nano Technology
Lawrence Livermore National Laboratory
Livermore, USA
lgoddard@gmail.com

Abstract—**We present a class of compact, monolithic, photonic sensors consisting of multiple section edge emitting lasers with functionalized lateral surface coatings for low level detection of chemical or biological agents. Specifically, we discuss 8μm x 250μm Pd-coated H_2 sensors and configurations to reduce the minimum detection limit from 138ppm for passive sensors to 1ppm for active sensors. Compared with conventional optical H_2 sensors that use fiber gratings, surface plasmon resonances, or surface reflectance, our sensors offer the advantages of smaller size, wider dynamic range, monolithic integration of laser source and detector, and 2-D scalability to arrays of sensors that are functionalized to detect different agents.**

I. INTRODUCTION

Our goal is to develop chip-scale sensor networks to detect and analyze unknown chemical and biological agents (CBAs) in-situ. Traditional optical sensors [1-6] already offer excellent sensitivity and specificity, but are generally difficult to miniaturize, integrate, or array. Fig. 1 shows the layout for our generic class of enhanced sensors. The sensor is a multiple section 2μm x 250μm edge emitting laser (EEL) with a 50nm thick Pd surface coating that is located 100nm above the active region and extends 3μm laterally on either side. Thus, the total sensor width is 8μm. The optical mode has a small overlap, $\Gamma_{Pd} \approx 1 \times 10^{-4}$, with this thin coating.
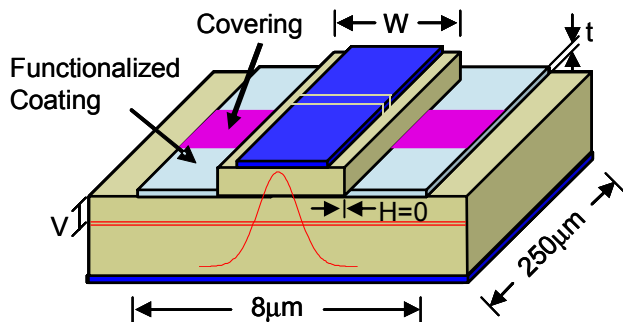

Figure 1. Multiple section laser with Pd coating for H_2 sensing shown with key design dimensions. A sensor array with various cover lengths enables compensation for system drift or temperature/current fluctuations.

As specific CBAs adsorb on the surface coating, the coating's optical properties change. In particular, both the extinction coefficient, κ, and the real part of the refractive index, n_r, decrease. H_2 gas reacts with Pd to form PdH thereby reducing the internal loss seen by the laser mode, α_i, from 58cm^{-1} at a rate of 0.03cm^{-1} per 100ppm of H_2 for our example sensor. Thus, the laser's output power increases rapidly in response to the amount of adsorbed H_2.

II. SENSOR DESIGN

A. Epitaxial structure

The sensors use a standard double quantum well (DQW) graded index separate confinement heterostructure (GRINSCH) with a graded doping profile as described in Table I. Lasers without lateral surface coatings have been previously fabricated and thoroughly characterized and modeled [7]. The laser wavelength varies from 950-970nm depending on bias and temperature.

Instead of cleaving laser facets, we etched vertical walls using an Electron Cyclotron Resonance (ECR) plasma etch [8]. This will enable scalability to 2-D sensor arrays and monolithic integration of optical sensors and photodetectors.

TABLE I. EPITAXIAL GROWTH LAYERS

Layer #	Material Type	Alloy (x,y)	T (μm)	Doping (cm^{-3})	Type	Dopant
16	GaAs		0.02	1.6E+19	p+	Zn
15	GaAs		0.18	1.7E+18	p	Zn
14	Al(x)GaAs	0.2	0.2	2E+18	p	Zn
13	Al(x)GaAs	0.6->0.2	0.2	0.3->2E+18	p	Zn
12	Al(x)GaAs	0.6	1	2.8E+17	p	Zn
11	Al(x)GaAs	0.11->0.6	0.2	-	UD	-
10	Al(x)GaAs	0.11	0.01	-	UD	-
9	GaIn(y)As	0.11	~0.0115	-	UD	-
8	Al(x)GaAs	0.11	0.015	-	UD	-
7	GaIn(y)As	0.1	~0.0115	-	UD	-
6	Al(x)GaAs	0.11	0.01	-	UD	-
5	Al(x)GaAs	0.6->0.11	0.2	5E16->3E17	n	Si
4	Al(x)GaAs	0.6	1	2E+17	n	Si
3	Al(x)GaAs	0.2->0.6	0.2	2E17->2E18	n	Si
2	Al(x)GaAs	0.2	0.2	2E+18	n	Si
1	GaAs		0.25	2E+18	n	Si
	GaAs Substrate				n+	

B. Modeling

The overlap of the laser field with the lateral surface coating, Γ_{Pd}, is the dominant factor affecting detector sensitivity. A small overlap yields a weak sensor since the resulting change in the internal loss will be small and so the output power will barely change. If the overlap is too large, the device simply will not lase. The four main fabrication parameters that determine the overlap are the ridge width, W, the Pd thickness, t, the horizontal distance from Pd to ridge, H, and the vertical distance from Pd to DQW, V (see Fig. 1). It is clear that increasing the horizontal distance reduces the overlap so we will assume H=0 for maximum sensitivity. The mode profile depends on the ridge height, which is set by the Pd to DQW distance, so we will allow V to vary.

The fundamental mode profiles and complex refractive indices were calculated using the beam propagation method (BPM), for three ridge widths: W=2μm, 5μm, and 10μm, six vertical separations: V=0nm to 500nm in 100nm increments, and eleven Pd thicknesses: t=0nm to 100nm in 10nm increments. The vertical separation is measured from the top QW (i.e. top of layer 9) to the bottom of the Pd coating. We assumed that the refractive index of the Pd layer at 950nm is comparable to the values at 835nm of 1.62+4.32j for unhydrided Pd and 1.45+3.86j in 4% hydrogen [3] and that the values are independent of Pd thickness. Also, we linearly interpolated for intermediate hydrogen concentrations. These three assumptions will need experimental verification.

Fig. 2 shows the typical pear shaped mode profile for the case W=2μm, V=100nm, and t=50nm. Inset shows t=0nm. Both have elliptical central field contours, but the contours at the field tails for t=50nm are significantly squeezed in by the Pd coating despite the tiny overlap. For W=5μm and 10μm (not shown), all contour lines were nearly elliptical.

We obtained the internal loss from the complex refractive index. Figs. 3a and 3b show the dependence of the internal loss on Pd thickness for W=2μm and 5μm, respectively.

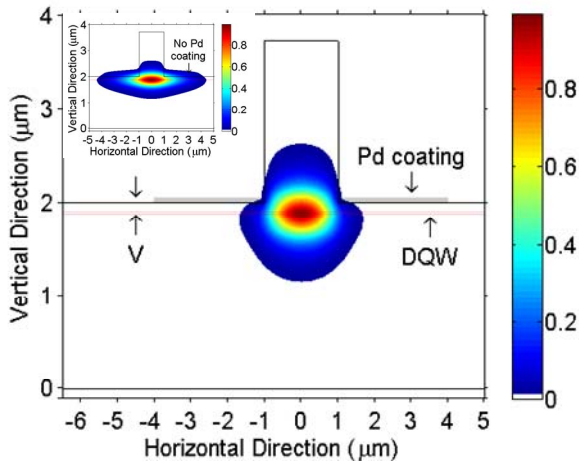Figure 2. Contour plot of the normalized electric field for W=2μm, V=100nm, and t=50nm. Inset shows W=2μm, V=100nm, and t=0nm. The 50nm thick Pd coating greatly squeezes in the mode.
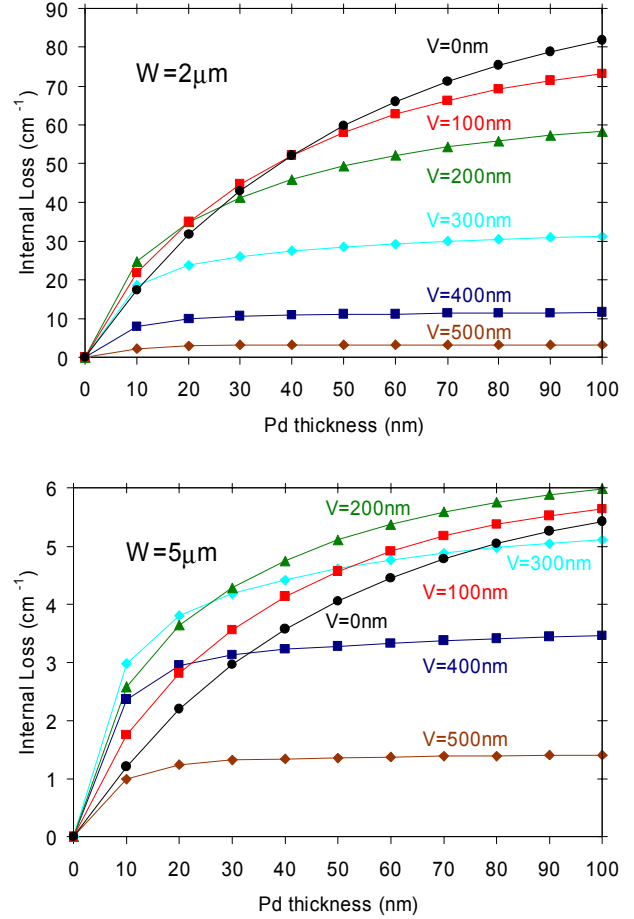

Figure 3. Internal loss versus Pd thickness for various vertical separations for (a) W=2μm and (b) W=5μm.

It is clear in all cases that the internal loss increases with Pd thickness, t, and that it eventually saturates since the field intensity decreases in the vertical direction. The dependence on vertical separation, V, is more complicated since this parameter is linked to the ridge etch depth. In Fig 3a, we see that for W=2μm and t≥40nm, the internal loss increases monotonically as V decreases to zero, i.e. the coating is brought closer to the DQW. For W=2μm and t≤40nm, the maximum internal loss occurs when V is a few hundred nanometers. This is because the shallower ridge etch leads to a wider mode and more lateral spreading into the Pd coating. For W=5μm, the separation that gives the maximum loss frequently changes with Pd thickness because of the tradeoff between mode size and proximity of the coating to the DQW. For t<30nm, the optimal V is 300nm, whereas for t between 30nm and 100nm, the optimal V is 200nm. In any event, the maximum loss for the W=5μm case is one order of magnitude lower than for the W=2μm case. The loss for W=10μm (not shown) case was two orders of magnitude lower. Thus, our sensor design is very versatile since a few sensors with slightly different ridge widths can measure an extremely wide dynamic range of H_2 concentrations.

Mode profiles and their internal losses were calculated for five H_2 concentrations: 0ppm to 400ppm in 100ppm increments for a subset of geometries: W=2µm and 5µm, V=0nm to 500nm in 100nm increments, and t=50nm and 100nm. The key figure of merit (FOM) is

$$FOM = -\Delta\alpha_i[1/((r-1)\Gamma g_0)+1/(\alpha_i+\alpha_m)], \qquad (1)$$

for a given change in H_2 concentration, e.g. 100ppm, since it equals the fractional change in EEL output power far above threshold. $\Gamma=0.072$ is the confinement factor, $g_0=1800cm^{-1}$ is the gain coefficient in the logarithmic gain model, $r\equiv I/I_{th}$ is the bias point, and $\alpha_m=45cm^{-1}$ is the mirror loss. Equation (1) is not valid near threshold. $\Delta P/P$ is much larger than the FOM due to the nonlinear L-I response in the laser knee.

Fig. 4 shows this FOM as a function of the vertical separation for the two Pd thicknesses. Assuming that the mode profile is unaltered in the presence of H_2, Γ_{Pd} would be constant and so we would expect $\Delta\alpha_i=\Gamma_{Pd}(4\pi\Delta\kappa/\lambda)$, since we linearly interpolated κ. This expected relationship is shown as the bottom two curves. Since H_2 reduces both κ and n_r in the Pd layer, there is a tradeoff. Reducing κ allows the mode to spread out more into the Pd layer, increasing Γ_{Pd}, and weakening $\Delta\alpha_i$. Reducing n_r squeezes the mode more strongly into the pear shape. The mode is pushed down and in thereby reducing Γ_{Pd} and strengthening $\Delta\alpha_i$. When the Pd layer is close to the DQW, the second effect is stronger. For our example sensor with V=100nm and t=50nm, the FOM was 1.87x larger than expected. The maximum enhancement of 2.26x occurred for V=0nm and t=100nm. As the ridge etch depth gets shallower and the vertical separation increases, the first effect becomes dominant and so the FOM decreases. Beyond 300nm separation, the FOM is less than expected. In summary, $\Delta\alpha_i$ depends on changes in both κ and the mode profile: $\Delta\alpha_i=\Gamma_{Pd}(4\pi\Delta\kappa/\lambda)+\Delta\Gamma_{Pd}(4\pi\kappa/\lambda)$.

C. Performance Simulations

We define the sensor's minimum detection limit (MDL) as the amount of CBA needed to produce a fractional change of the sensor output power, $\Delta P/P$, of 10^{-3}. Typical fluctuations in the output power from temperature and current biasing instabilities and from the laser's natural relative intensity noise (RIN) are at least one order of magnitude smaller than this. Laser RIN is greatest at threshold and decreases rapidly just above threshold. Thus, for optimal MDL, the sensor should be operated at or just above the laser threshold knee, $r\approx1$, so that P is small and the RIN is not too large. Also, differential measurements on an array of sensors should be made to compensate for drift and temperature or current fluctuations. Using equation (1), the MDL in ppm is approximately given as 0.1/FOM for r>>1.

A 1-D rate equation model, previously verified against experimental L-I data [7], was used to calculate the response (see Fig. 5) for L=250µm, W=2µm, V=100nm, and t=50nm for three types of Pd-coated sensors: a passive waveguide (WG), a single section EEL, and a multiple section EEL that has a 37.5µm long unbiased saturable absorber as the center section of Fig. 1. For a fair comparison, we adjust the biases so that the sensor's output optical power is fixed at 10µW for zero H_2. The predicted MDLs of the structures were 138ppm, 4ppm, and 1ppm, respectively. The passive WG requires 43µW of input optical power, whereas the EELs need no input optical power but use 8mW and 13mW, respectively, of electrical power, given the operation voltage of 1.5V. Shorter cavity lengths used less power but had higher MDLs. The resonant cavity of the EEL provides a strong nonlinearity in the sensor response, i.e. the lasing knee, and thereby reduced the MDL compared to the passive WG. The saturable absorber further amplifies this lasing knee nonlinearity according to the gain lever effect [9, 10]. The gain lever effect has been shown to enhance the amplitude modulation efficiency by 30-40dB [10] and yield lasers with greater than unity external quantum efficiencies [9, 10].
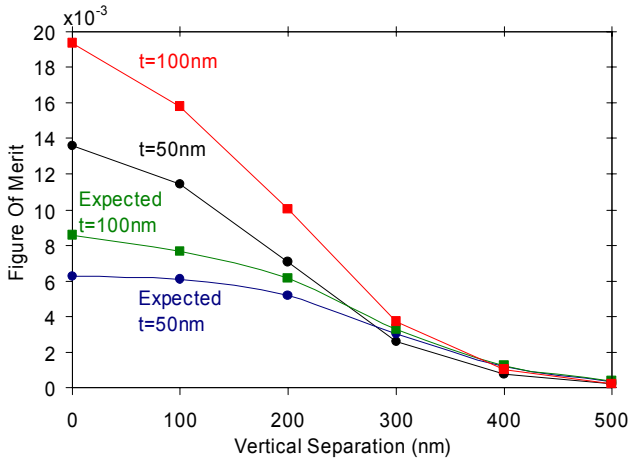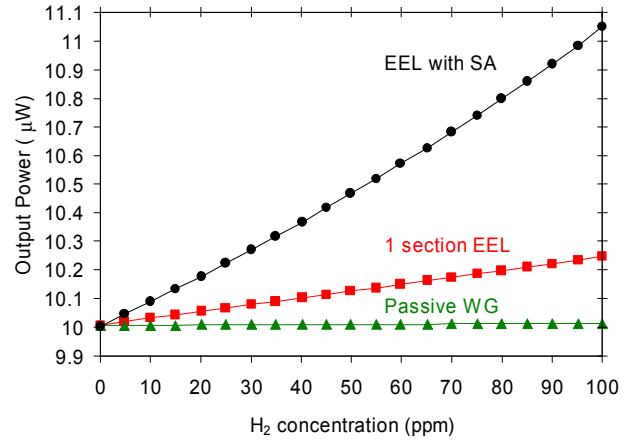
Figure 4. Figure of merit versus vertical separation for two thicknesses of Pd, assuming r=1.02 and a 100ppm change in H_2 concentration. The expected value curves assume that H_2 does not change the mode profile.

Figure 5. Simulated sensor responses for Pd coated passive WG, single section EEL, and multi-section EEL with 15% saturable absorber for W=2µm, V=100nm, and t=50nm. P_{out} increases since H_2 reduces α_i.
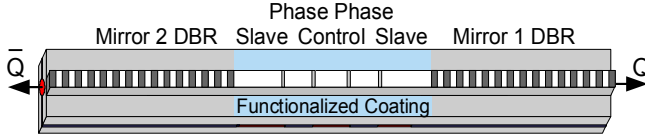
Figure 6.   Functionalized enhanced photonic sensor with threshold detection. H_2 reduces α_i, shifts the phase, and swaps the output facet.

D.   Further Enhancements

Fig. 6 shows another class of generic sensors for higher sensitivity wider dynamic range threshold detection. The multiple section EEL with lateral coatings is embedded inside slightly detuned DBR mirrors. As before H_2 reduces α_i and increases the circulating power, P_{circ}, which reduces the average carrier density, N_{avg}, due to increased stimulated emission. This shifts the round-trip cavity phase. The phase shift is enhanced in multiple section EELs according to the gain-index lever [11] (see Fig. 7a). The cavity length is chosen such that the spacing of wavelengths satisfying the round-trip phase condition is 1-2% smaller than the spacing of the gain peaks from the detuned DBR mirrors. This creates a Vernier effect (see Fig. 7b), which magnifies the phase shift [11] caused by the presence of H_2. When the H_2 concentration increases above an electronically controllable threshold, the laser hops from λ_1 to λ_2. The special DBR mirrors [11] (see Fig. 8) have highly reflective (HR) and antireflective (AR) facets that are reversed for λ_1 and λ_2. Thus, above the given H_2 threshold, the output facet swaps. Adjusting the biases on the slave and control sections changes the gain-index lever strength and allows coarse electronic control of this H_2 threshold. Adjusting the phase section bias allows fine electronic control. If the phase in the absence of H_2 is set near the mode hop point, an extremely low MDL can be achieved, limited only by the stability of the drive currents and ambient environmental conditions.

III.   Conclusions

Functionalized lateral surface coated in-situ CBA sensors were presented and analyzed. These chip-scale sensors offer high sensitivity, wide dynamic range, inline integration with photodetectors, and 2-D scalability for drift compensation and for detection and identification of multiple CBAs.
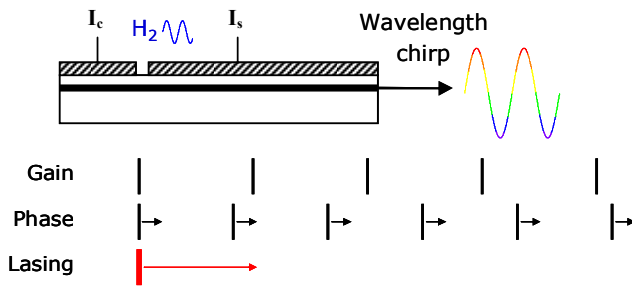

Figure 7.   (a) The gain-index lever in multiple section lasers is used to enhance the phase shift caused by the decrease in N_{avg} due to H_2. (b) The next mode is aligned using the Vernier effect, which magnifies the shift.
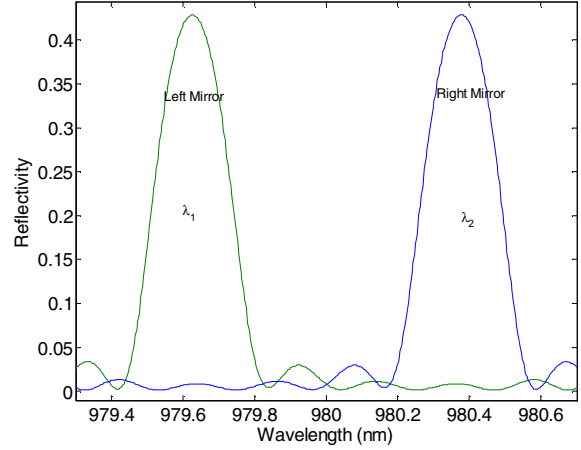

Figure 8.   Desired reflectivity profile for an alternating facet laser. At λ_1, the left mirror is HR and the right is AR so laser light exits the right facet. H_2 causes the mode to hop to λ_2 and switches the light to the left facet.

For maximal sensitivity, a large field overlap with the coating is needed. This can be achieved with a narrow ridge, a thick coating layer, zero horizontal distance between ridge and coating, and a small vertical separation between coating and active region. For the 8μm x 250μm H_2 sensor with W=2μm, V=100nm, t=50nm, a MDL of 1ppm is predicted.

References

[1]   C. Christofides and A. Mandelis, "Solid-state sensors for trace hydrogen detection," *J. Appl. Phys.*, vol. **68**, pp. R1-R30, 1990.

[2]   A. Mandelis and J. Garcia, "Pd/PVDF thin film hydrogen sensor based on laser-amplitude-modulated optical-transmittance: dependence on H_2 concentration and device physics," *Sens. Act. B*, vol. **49**, pp. 258-267, 1998.

[3]   P. Tobiska, O. Hugon, A. Trouillet, and H. Gagnaire, "An integrated optic hydrogen sensor based on SPR on palladium," *Sens. Act. B*, vol. **74**, pp. 168-172, 2001.

[4]   S. James and R. Tatum, "Optical fibre long-period grating sensors: characteristics and application," *Meas. Sci. Technol.*, vol. **14**, pp. R49-R61, 2003.

[5]   J. Villatoro, A. Diez, J. Cruz, and M. Andres, "In-line highly sensitive hydrogen sensor based on palladium-coated single-mode tapered fibers," *IEEE Sens. J.*, vol. **3**, pp. 533-537, 2003.

[6]   Z. Zhao, M. Carpenter, H. Xia, and D. Welch, "All-optical hydrogen sensor based on a high alloy content palladium thin film," *Sens. Act. B.*, vol. **113**, pp. 532-538, 2006.

[7]   M. Pocha, L. Goddard, T. Bond, R. Nikolic, S. Vernon, J. Kallman, et al., "Electrical and optical gain lever effects in InGaAs double quantum well diode lasers," *IEEE J. Quantum Electron.*, in press.

[8]   R. Welty, T. Bond, E. Behymer, M. Pocha, G. Loomis, J. Wolfe, et al., "Integrated laser with low-loss high index-contrast waveguides for OEICs," in *Proc. SPIE*, vol. **5729**, pp. 49-60, 2005.

[9]   K. Vahala, M. Newkirk, and T. Chen, "The optical gain lever: A novel gain mechanism in the direct modulation of quantum well semiconductor lasers," *Appl. Phys. Lett*, vol **54**, pp. 2506-2508, 1989.

[10]   N. Moore and K. Lau, "Ultrahigh efficiency microwave signal transmission using tandem-contact single quantum well GaAlAs lasers," *Appl. Phys. Lett.,* vol. **55**, pp. 936-938, 1989.

[11]   L. Goddard, J. Kallman, and T. Bond, "Rapidly reconfigurable all-optical universal logic gates," *Proc. SPIE*, vol. **6368**, pp. 63680H-1-13, 2006.